AGU PUBLICATIONS

JGR

Journal of Geophysical Research: Atmospheres

RESEARCH ARTICLE
10.1002/2014JD021642

Key Points:
- The structure of the Hadley Circulation is important to cloud change
- Intermodel spreads in circulation and cloud feedbacks are well correlated
- Better performing models in moist dynamics have high climate sensitivity

Correspondence to:
H. Su,
Hui.Su@jpl.nasa.gov

Citation:
Su, H., J. H. Jiang, C. Zhai, T. J. Shen, J. D. Neelin, G. L. Stephens, and Y. L. Yung (2014), Weakening and strengthening structures in the Hadley Circulation change under global warming and implications for cloud response and climate sensitivity, *J. Geophys. Res. Atmos.*, *119*, 5787–5805, doi:10.1002/2014JD021642.

Received 12 FEB 2014
Accepted 26 APR 2014
Accepted article online 4 MAY 2014
Published online 20 MAY 2014

Weakening and strengthening structures in the Hadley Circulation change under global warming and implications for cloud response and climate sensitivity

Hui Su[1], Jonathan H. Jiang[1], Chengxing Zhai[1], Tsaepyng J. Shen[1], J. David Neelin[2], Graeme L. Stephens[1], and Yuk L. Yung[3]

[1]Jet Propulsion Laboratory, California Institute of Technology, Pasadena, California, USA, [2]Department of Atmospheric and Oceanic Sciences, University of California, Los Angeles, California, USA, [3]Division of Geological and Planetary Sciences, California Institute of Technology, Pasadena, California, USA

Abstract It has long been recognized that differences in climate model-simulated cloud feedbacks are a primary source of uncertainties for the model-predicted surface temperature change induced by increasing greenhouse gases such as CO_2. Large-scale circulation broadly determines when and where clouds form and how they evolve. However, the linkage between large-scale circulation change and cloud radiative effect (CRE) change under global warming has not been thoroughly studied. By analyzing 15 climate models, we show that the change of the Hadley Circulation exhibits meridionally varying weakening and strengthening structures, physically consistent with the cloud changes in distinct cloud regimes. The regions that experience a weakening (strengthening) of the zonal-mean circulation account for 54% (46%) of the multimodel-mean top-of-atmosphere (TOA) CRE change integrated over 45°S–40°N. The simulated Hadley Circulation structure changes per degree of surface warming differ greatly between the models, and the intermodel spread in the Hadley Circulation change is well correlated with the intermodel spread in the TOA CRE change. This correlation underscores the close interactions between large-scale circulation and clouds and suggests that the uncertainties of cloud feedbacks and climate sensitivity reside in the intimate coupling between large-scale circulation and clouds. New model performance metrics proposed in this work, which emphasize how models reproduce satellite-observed spatial variations of zonal-mean cloud fraction and relative humidity associated with the Hadley Circulation, indicate that the models closer to the satellite observations tend to have equilibrium climate sensitivity higher than the multimodel mean.

1. Introduction

On global average, clouds exert a net cooling effect of about $-21.1 \pm 5\ \mathrm{W\,m^{-2}}$ at the top of atmosphere (TOA) [*Stephens et al.*, 2012] as their reflection of solar radiation overcomes their trapping of terrestrial emission. Compared to the radiative forcing induced by the doubling of atmospheric CO_2 concentration, about $4\ \mathrm{W\,m^{-2}}$, any changes in cloud amount, cloud optical thickness, or cloud top temperature would greatly modulate the radiative balance of the Earth system, causing large differences in the model-predicted global-mean surface temperature increase [*Cess et al.*, 1989; *Stephens*, 2005]. A commonly used measure for climate response is equilibrium climate sensitivity (ECS), defined as equilibrium global-mean surface air temperature change in response to a sustained doubling of CO_2 relative to the preindustrial concentration. Based on the coupled atmospheric-ocean model simulations submitted to the Coupled Model Intercomparison Project Phase 5 (CMIP5), ECS ranges from 2.1 to 4.7 K [*Andrews et al.*, 2012]. Differences in simulated cloud radiative effect (CRE) changes in response to increasing CO_2 and associated cloud feedbacks are a primary source for the uncertainty of ECS estimates [e.g., *Cess et al.*, 1989; *Andrews et al.*, 2012]. Understanding the physical processes that drive CRE changes and identifying the dominant contributor to the intermodel differences in CRE changes and cloud feedbacks are of critical importance for reducing the spread of ECS.

Cloud distributions and variations are intimately linked to large-scale circulation [e.g., *Hartmann and Michelsen*, 1993; *Bony et al.*, 2004; *Bony and Dufresne*, 2005; *Su et al.*, 2008, 2013], while cloud radiative effects may also impact regional and global energy balance and modulate large-scale circulation [e.g., *Frierson and Hwang*, 2012; *Hwang and Frierson*, 2013; *Loeb et al.*, 2014]. *Stevens and Bony* [2013] stressed that "a deeper understanding and

better representation of the coupling between water and circulation" is "necessary to reduce the uncertainty in estimates of the climate sensitivity."

Simple thermodynamic arguments suggest that the tropical overturning circulation would slow down under global warming [*Held and Soden*, 2006]. Neglecting the energy transport between the tropics and extratropics, the primary energy balance averaged over the tropics is between radiative cooling and convective heating. When surface temperature increases, atmospheric water vapor increases at approximately 7% per degree increase of temperature following the Clausius-Clapeyron relation. The increase of tropical average precipitation follows the rate of radiative cooling increase, at about 2%/K [*Stephens and Ellis*, 2008]. Therefore, convective mass flux and large-scale ascent must slow down on large spatial averages. Consistently, atmospheric dry static stability ($\sigma = \frac{\partial \theta}{\partial p}, \theta$ being potential temperature) increases faster than the increase of radiative cooling rate with temperature [*Knutson and Manabe*, 1995], leading to the weakening of large-scale subsidence. Such theoretical predictions are applicable to both the Hadley Circulation and the Walker Circulation, although a greater decreasing trend is found in the Walker Circulation than in the Hadley Circulation in the model simulations and observations [*Held and Soden*, 2006; *Vecchi and Soden*, 2007]. The change of the sea surface temperature (SST) gradient in the tropical Indo-Pacific region may also contribute to the slowing down of the Walker Circulation [*Tokinaga et al*., 2012]. Although observational evidence for the weakening of tropical circulation has been controversial [*Mitas and Clement*, 2005; *Quan et al*., 2004; *Nguyen et al*., 2012; *Wang et al*., 2013], most climate model simulations predict an overall weakening of tropical circulation under the doubled CO_2 scenario by measures that emphasize large spatial scales [*Vecchi and Soden*, 2007; *Lu et al*., 2007; *Bony et al*., 2013].

The weakening of the Hadley Circulation is often measured by the maximum mass-weighted zonal-mean meridional stream function or velocity potential at a particular pressure level [*Oort and Yienger*, 1996; *Tanaka et al*., 2004], or by the variances or fractional changes of vertical velocity averaged over the tropics [*Held and Soden*, 2006; *Bony et al*., 2013]. For example, the spatial structures of the Hadley Circulation change under global warming are analyzed in terms of the zonally integrated meridional stream function in *Ma et al*. [2012] and *Ma and Xie* [2013]. The detailed structures in zonal-mean vertical velocity profiles have not been studied extensively. The model-simulated vertical velocity change under doubled CO_2 scenario exhibits more than a simple weakening of the Hadley Circulation. Acceleration and deceleration occur within each ascending or descending branch of the Hadley Circulation [*Richter and Xie*, 2008]. In addition, upward and poleward expansion of the Hadley Circulation edges are found in the models [*Lu et al*., 2007]. A recent study by *Bony et al*. [2013] showed that at least half of the tropical regional precipitation change at the end of the 21st century, under the projected quadrupling of CO_2 (a scenario without any mitigation of anthropogenic emission), would be contributed by the large-scale circulation change. The model spread in the dynamic component of precipitation changes plays a predominant role in the model spread of regional precipitation pattern. How are the complex structures of the Hadley Circulation change related to the cloud response to global warming? Are the magnitudes of the Hadley Circulation change correlated with the CRE changes, cloud feedbacks, and climate sensitivity? Do circulation and clouds vary independently or coherently? We address these questions using 15 climate model simulations that were submitted to the CMIP5. Satellite observations and reanalysis data are used to evaluate model performance in representing the Hadley Circulation and cloud structures.

Section 2 describes the model simulations and satellite data. Section 3 provides a detailed account of the physical linkage between the Hadley Circulation and cloud changes from present day in one of the projected warming scenarios, the Representative Concentration Pathway (RCP) 4.5. Section 4 quantifies the relationships between the model-simulated Hadley Circulation change and TOA CRE change. Caveats of the analysis are discussed in section 5. In section 6, new metrics that evaluate the model performance are proposed, along with their implications for ECS. Concluding remarks are summarized in section 7.

2. Models and Data

We use 15 coupled atmosphere-ocean models from the CMIP5 archive whose ECS and vertical profiles of winds, clouds, and relative humidity in both present-day climate and in the RCP 4.5 scenario were available at the time of the analysis (Table 1). Most ECS values are taken from *Andrews et al*. [2012] based on the linear regression analysis of the instantaneous quadrupling of CO_2 experiments. The ECSs for NCAR cam5 and GISS e2r are not provided in *Andrews et al*. [2012] but obtained from *Shindell et al*. [2013]. The ECSs for the 15

Table 1. Atmosphere-Ocean Coupled CMIP5 Models Used in This Study and Corresponding Equilibrium Climate Sensitivity Based on *Andrews et al.* [2012] and *Shindell et al.* [2013]

Modeling Center	Acronym	Model Name	Resolution	ECS (K)
Canadian Centre for Climate Modeling and Analysis, Canada	CCCMA	canesm2	2.8125° × 2.7673°, L35	3.69
Centre National de Recherches Météorologiques, France	CNRM[a]	cm5[a]	1.4° × 1.4°, L31	3.25
Commonwealth Scientific and Industrial Research Organization/Queensland Climate Change Centre of Excellence, Australia	CSIRO-QCCCE	mk3.6	1.9° × 1.9°, L18	4.08
Geophysical Fluid Dynamics Laboratory, USA	GFDL	cm3	2.5° × 2°, L48	3.97
Geophysical Fluid Dynamics Laboratory, USA	GFDL	esm2g		2.39
Goddard Institute for Space Studies, USA	GISS	e2-r	2.5° × 2°[b], L29	2.11
Institute for Numerical Mathematics, Russia	INM	cm4	2° × 1.5°, L21	2.08
Institut Pierre Simon Laplace, France	IPSL	cm5a	3.75° × 1.8947°, L39	4.13
Model for Interdisciplinary Research On Climate/Atmos. Ocean Res. Ins., U. Tokyo/Nat. Ins. Env. Std./Japan Agency for Marine-Earth Sci. & Tech., Japan	MIROC	miroc5	0.5625° × 0.55691°, L56; 1.4° × 1.4°, L40	2.72
Model for Interdisciplinary Research On Climate/Atmos. Ocean Res. Ins., U. Tokyo/Nat. Ins. Env. Std./Japan Agency for Marine-Earth Sci. & Tech., Japan	MIROC	miroc-esm	0.56250.55691, L56; 1.4° × 1.4°, L40	4.67
Max Planck Institute	MPI	esm-lr	1.875° × 1.875°, L47	3.63
Meteorological Research Institute, Japan	MRI	cgcm3	1.125° × 1.1121°, L48	2.60
National Center for Atmospheric Research, USA	NCAR	cam5	1.25° × 0.9424°, L30	4.10
Norwegian Climate Center (NCC), Norway	NCC	noresm	2.5° × 1.8947°, L26	2.80
UK Met Office Hadley Climate Center, UK	MOHC	hadgem2-es	1.875° × 1.25°, L38	4.59

[a]CNRM CM5 does not provide cloud fraction profiles in the historical run.
[b]GISS e2-r resolution was incorrectly listed as 5° × 4°, in *Jiang et al.* [2012, Table 1].

models range from 2.1 to 4.7 K (Table 1), with a multimodel mean of 3.4 K. Eight models are categorized as high-sensitivity models with ECS greater than 3.4 K, while seven models with ECS lower than 3.4 K are categorized as low-sensitivity models.

We use the 1980–2004 averages from the historical runs to represent the present-day climate and the 2074–2098 averages from the RCP 4.5 runs to represent a projected warmer climate. The RCP 4.5 run [*Taylor et al.*, 2012] corresponds to a scenario with moderate mitigation efforts such that the CO_2 concentration reaches 538 ppmv in 2100 and smoothly approaches a constant of 543 ppmv by 2150 onward, corresponding to an approximate doubling of the preindustrial CO_2 concentration of 278 ppmv [*Meinshausen et al.*, 2011]. The projected radiative forcing aims at 4.5 W m^{-2} by 2100; however, the adjusted radiative forcings taking into account rapid cloud adjustments to forcings are in fact different among the models, ranging from 2.8 to 4.7 W m^{-2} in 2095 with the multimodel mean below 4.5 W m^{-2} [*Meinshausen et al.*, 2011; *Forster et al.*, 2013]. The external forcings in the RCP 4.5 runs include not only the increase of CO_2 and other greenhouse gases, but also the decrease of aerosols, recovery of stratospheric ozone, and changes in land surface. Thus, the projected climate changes in RCP 4.5 may have characteristics different from the runs with only CO_2 changes. The climate "changes" in this study are referred to as the differences between the two 25 year averages, i.e., the averages of 2074–2098 in the RCP 4.5 scenario minus the averages of 1980–2004. The detailed model performances in simulating present-day water vapor and clouds are referred to *Jiang et al.* [2012].

In this study, the vertical profiles of cloud fraction are analyzed as the primary indicator of cloud properties, as cloud optical thickness often varies consistently with cloud fraction [*Zelinka et al.*, 2013] and cloud top height variations can be approximately inferred from the changes in cloud fraction profiles. In cases in which the variations of cloud optical thickness and cloud fraction changes are out of phase, our analyses may not provide a complete description of the associated CRE changes. A comprehensive analysis of the relative contributions of cloud fraction, cloud optical thickness, and cloud top height changes to rapid cloud adjustments and cloud feedbacks can be found in *Zelinka et al.* [2013].

Observed cloud fraction data are taken from CloudSat/CALIPSO joint retrievals (2B-CLDCLASS-LIDAR, version R04) from June 2006 to December 2010 [*Mace et al.*, 2009]. The uncertainty of CloudSat/CALIPSO cloud

fraction measurements is about 5% [*Mace et al*., 2009]. Ideally, model outputs of CloudSat/CALIPSO simulator cloud fraction should be used for comparison with the satellite retrievals [*Bodas-Salcedo et al*., 2011; *Su et al*., 2013]. As most of the models do not produce CloudSat/CALIPSO simulator cloud fraction outputs, we assume additional 20% uncertainty when comparing the model cloud fraction with satellite data [*Su et al*., 2013].

We also examine relative humidity profiles in the models because of the strong correlation between cloud fraction and relative humidity as noted by previous studies [e.g., *Fasullo and Trenberth*, 2012]. The observed relative humidity measurements are taken from the Atmospheric Infrared Sounder (AIRS) on the Aqua satellite at pressure levels greater than 300 hPa and from the Microwave Limb Sounder (MLS) on the Aura satellite at pressure levels less than 300 hPa for the period of August 2004 to December 2012. AIRS relative humidity (version 6) has an uncertainty of about 10% [*Olsen et al*., 2013], while the MLS relative humidity (version 3) has an uncertainty of about 25% in the tropical upper troposphere [*Read et al*., 2007]. Hence, we assume a 25% uncertainty for the combined AIRS and MLS relative humidity measurements. Vertical pressure velocities from the European Centre for Medium-Range Weather Forecasts (ECMWF) interim reanalysis (ERA-interim) are used for comparison with model vertical winds.

3. Linkage Between the Meridional Structures of the Hadley Circulation Change and Cloud Change

The multimodel-mean zonal-mean vertical pressure velocity (ω) changes from the 15 models are shown in Figure 1a, with the climatological ω profiles superimposed as contours. Only the latitudes from 45°S to 40°N within the Hadley Circulation boundaries are shown. It is true that the signs of the ω change oppose those of the climatological ω over many latitudinal zones, corresponding to a weakening of the circulation. However, there are latitudinal bands where the ω changes are of the same sign as the climatological ω, including the equatorial region (~5°S to ~5°N) and the flanks of the descent zones (~30°N to ~40°N, ~15°S to ~20°S, and ~30°S to ~45°S), corresponding to a strengthening of the circulation. The latitudinally alternating positive and negative ω changes are also indicative of the shifts of the ascent and descent boundaries. In the upper troposphere and within the climatological ascending branch, a uniform increase of the upward motion marks the deepening of the troposphere and the upward expansion of the Hadley Circulation. All of these features underscore the complex structures in the response of the Hadley Circulation under global warming. We attempt to establish the linkage between the structures in the Hadley Circulation change and the clouds and TOA CRE changes in the RCP 4.5 scenario, as shown in Figures 1b and 1c, with particular attention to the underappreciated strengthening segments in the Hadley Circulation change. Zonal-mean relative humidity change is superimposed on the cloud fraction change in Figure 1b. Cloud radiative effect (CRE) is defined as the all-sky and clear-sky radiative flux differences with a positive sign representing a warming effect to the Earth-atmosphere system. In Figure 1c, a positive CRE change corresponds to an increase of cloud warming effect or a decrease of cloud cooling effect.

3.1. Changes Over the Ascending Branch of the Hadley Circulation

Within the ascending branch of the climatological Hadley cell, zonal-mean large-scale rising motion strengthens near the equator between ~5°S and ~5°N but weakens at the flanks around 5°–15°N/S, suggesting a narrowing of the tropical ascending zone. The weakening of large-scale ascent over the 5°–15°N/S latitude bands is a manifestation of the aforementioned theoretical prediction of the slowing down of the tropical circulation but shows that the slowing down required on large-scale averages can be met despite locally more intense changes of varying sign. The local weakening at the poleward flanks of the climatological ascending branch is consistent with the "upped-ante mechanism" [*Neelin et al*., 2003; *Chou and Neelin*, 2004], which suggests that the margins of the convective zones tend to experience reduced convection under global warming. In these regions, dry air inflow from adjacent nonconvective regions limits the increase of lower tropospheric moisture, making it more difficult to reach the values (the increased "convective ante") imposed by warmer troposphere temperature. The weakened ascending motion in the convective regions is associated with reduced deep convective clouds, evidenced by the greatest negative cloud fraction change in the upper troposphere and a secondary minimum in the middle troposphere around 600 hPa between 5° and 15°N/S (Figure 1b). The reduction of high-level and midlevel cloud amounts results in decreased longwave warming and shortwave cooling effects by clouds at the TOA (Figure 1c), leading to a relatively small net cloud warming effect within 5°–15°N/S because of the near cancellation between the longwave and shortwave CREs.

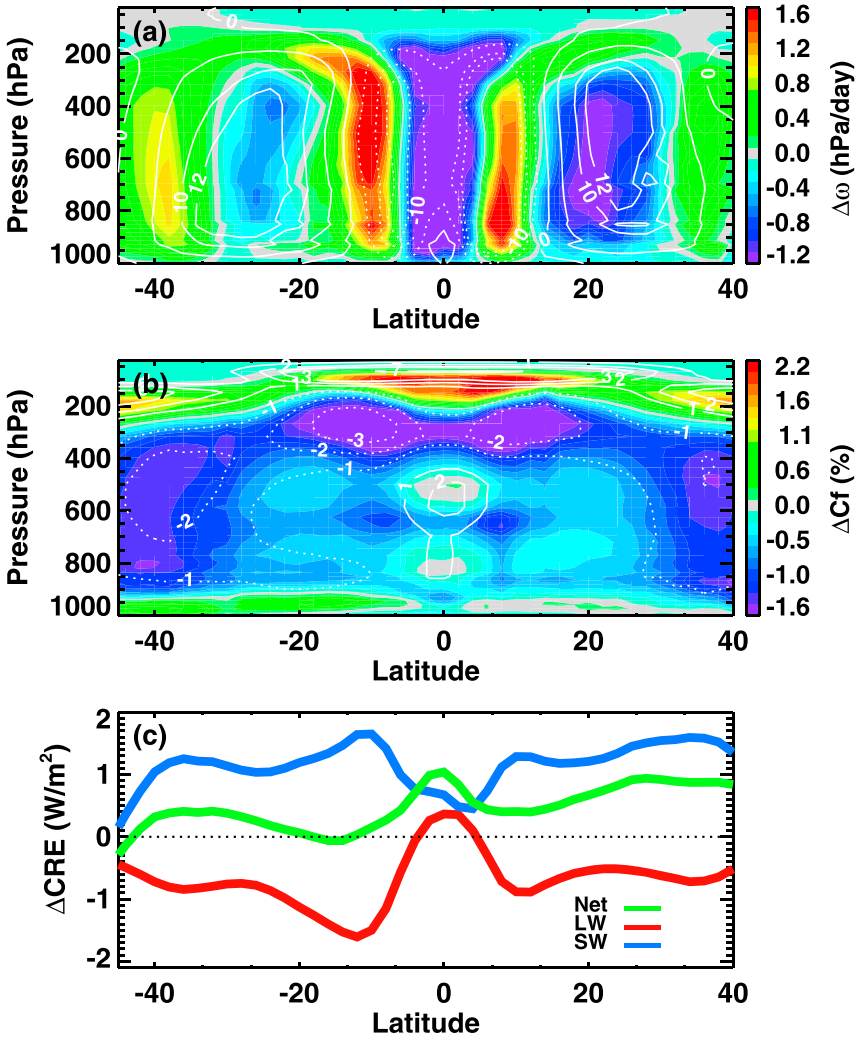

Figure 1. The multimodel-mean zonal-mean vertical pressure velocity (ω), cloud fraction (CF), relative humidity (RH), and cloud radiative effect (CRE) changes from the present day to the end of the 21st century projected in the RCP 4.5 scenario. (a) Changes of ω in color shadings and the present-day climatological ω in contours, (b) changes of CF in color shadings and RH in contours, and (c) changes of area-weighted top-of-atmosphere (TOA) net, longwave and shortwave CREs. The changes refer to the differences of each variable between the averages for 2074–2098 in the RCP 4.5 scenario and for 1980–2004.

On the other hand, the strengthened ascent within ~5°S to ~5°N may seem to be at odds with the general notion of slowing down of tropical circulation under global warming. This is because the simple energy balance and thermodynamic arguments for the tropical average [*Held and Soden*, 2006; *Knutson and Manabe*, 1995] are not applicable to the local regions where strong horizontal transport occurs. The increased boundary layer moist static energy associated with locally warmer surface temperature reduces the gross moist stability and enhances lower tropospheric moisture convergence and thus deep convection [*Neelin et al*., 2003; *Chou and Neelin*, 2004]. The increased upward velocity and dry static stability lead to increased adiabatic cooling, which has to be balanced by increased latent heating associated with stronger precipitation (shown in Figure 2). In the horizontal maps (Figures 3b–3d), the enhanced equatorial convection is concentrated over the equatorial Pacific Ocean with compensating subsidence to the east and west; therefore, only a small increase of cloud fraction and relative humidity is shown in the zonal mean from 850 to 400 hPa within 5°S–5°N (Figure 1b).

Above 400 hPa over the entire tropics, a dipole pattern of "positive above and negative below" in the cloud fraction and relative humidity changes suggest a rising altitude of convective detrainment and cirrus cloud top, causing an increased longwave warming effect by clouds (Figure 1c). The dipole pattern of high-level

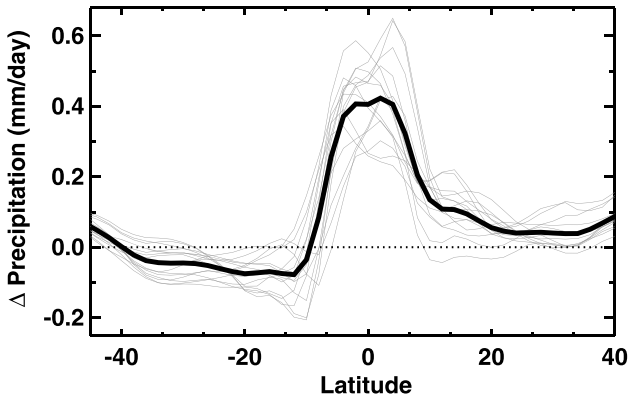

Figure 2. The area-weighted zonal-mean precipitation change from the present day to the end of the 21st century projected in the RCP 4.5 scenario for the multimodel mean (thick black curve) and 15 CMIP5 models (thin gray curves).

cloud change is clear evidence of deeper penetration of convection and upward expansion of the Hadley Circulation. The rise of cirrus cloud top is consistent with the "fixed-anvil-temperature" hypothesis, which suggests that the convective detrainment temperature would be approximately constant under global warming [*Hartmann and Larson*, 2002; *Zelinka and Hartmann*, 2011]. It is a robust feature simulated by all climate models [*Zelinka et al*., 2013] and is associated with an increase of longwave warming effects by clouds. The combined effects of cloud altitude and cloud optical thickness increase and cloud fraction change result in a peak of increased longwave warming by clouds at the equator. In Figure 1c, only the equatorial band between ~5°N and ~5°S shows positive longwave CRE changes, partly because the cloud masking effects [*Soden et al*., 2004] would cause a systematic underestimate of the longwave cloud warming [*Soden et al*., 2008; *Zelinka et al*., 2013]. In kernel-derived cloud feedbacks, the longwave warming associated with the increasing cloud top height is positive over most of the globe [e.g., *Zelinka et al*., 2013].

3.2. Changes Over the Descending Branch of the Hadley Circulation

The latitudinal bands between 15° and 45°N/S are the climatological descent branches of the Hadley cell. The changes of large-scale subsidence are mostly evident between 40°N and 45°S. The ω changes exhibit undulating behaviors with weakening at most of the descent zones (15°N–30°N and 20S°–30°S) but strengthening at the edges (~30°N to ~40°N, ~15°S to ~20°S, and ~30°S to ~45°S). The weakening is more severe in amplitude in the northern hemisphere, while the strengthening is more expansive in the southern hemisphere.

The weakening of subsidence between 15° and 30°N/S is in concert with the weakening of rising motion over the climatological ascending zones, as predicted by simple theories. In these latitudinal bands, the dominant cloud types are marine stratocumulus and stratus as well as fair-weather cumulus and cirrus [*Tselioudis et al*., 2013]. A reduction of low cloud fraction is noticeable in the zonal mean between 800 and 900 hPa, co-located with a decrease of relative humidity (Figure 1b) and a weakening of large-scale subsidence (Figure 1a). The cause for the decrease of the subtropical low clouds is not known [*Bretherton et al*., 2013; *Blossey et al*., 2013]. A plausible mechanism suggested by *Sherwood et al*. [2014] involves the convective mixing between the free troposphere and the boundary layer. In this theory, the weakened subsidence under global warming promotes the deepening of the boundary layer [*Bretherton et al*., 2013; *Blossey et al*., 2013], allowing more entrainment of free tropospheric dry air into the boundary layer and leading to a decrease of low clouds [*Rieck et al*., 2012; *Stevens*, 2007; *Sherwood et al*., 2014].

Below 900 hPa, zonal-mean low cloud fraction shows a small increase (Figure 1b), especially in the southern subtropics. Increasing surface evaporation or lower tropospheric stability (LTS) might contribute to such an increase, although the exact mechanisms are not known.

The fair-weather cumulus and cirrus over the subtropical regions may originate from convective detrainment and occur near the convective margins [*Tselioudis et al*., 2013], such as at the edges of South Pacific Convergence Zone and in the subtropical North Pacific and North Atlantic (Figures 3c and 3d). The equatorward shift of deep convection within 5°–15°N/S and the poleward shift of midlatitude storm tracks may both contribute to the decrease of isolated cumulus and cirrus, coincident with a decrease in free tropospheric relative humidity (Figures 1b, 3c, and 3d).

The 15°–30°N/S latitude bands include monsoonal convection over land (such as Southeast Asia, North America, South America, and Africa). There are strong zonal asymmetries in atmospheric circulation and

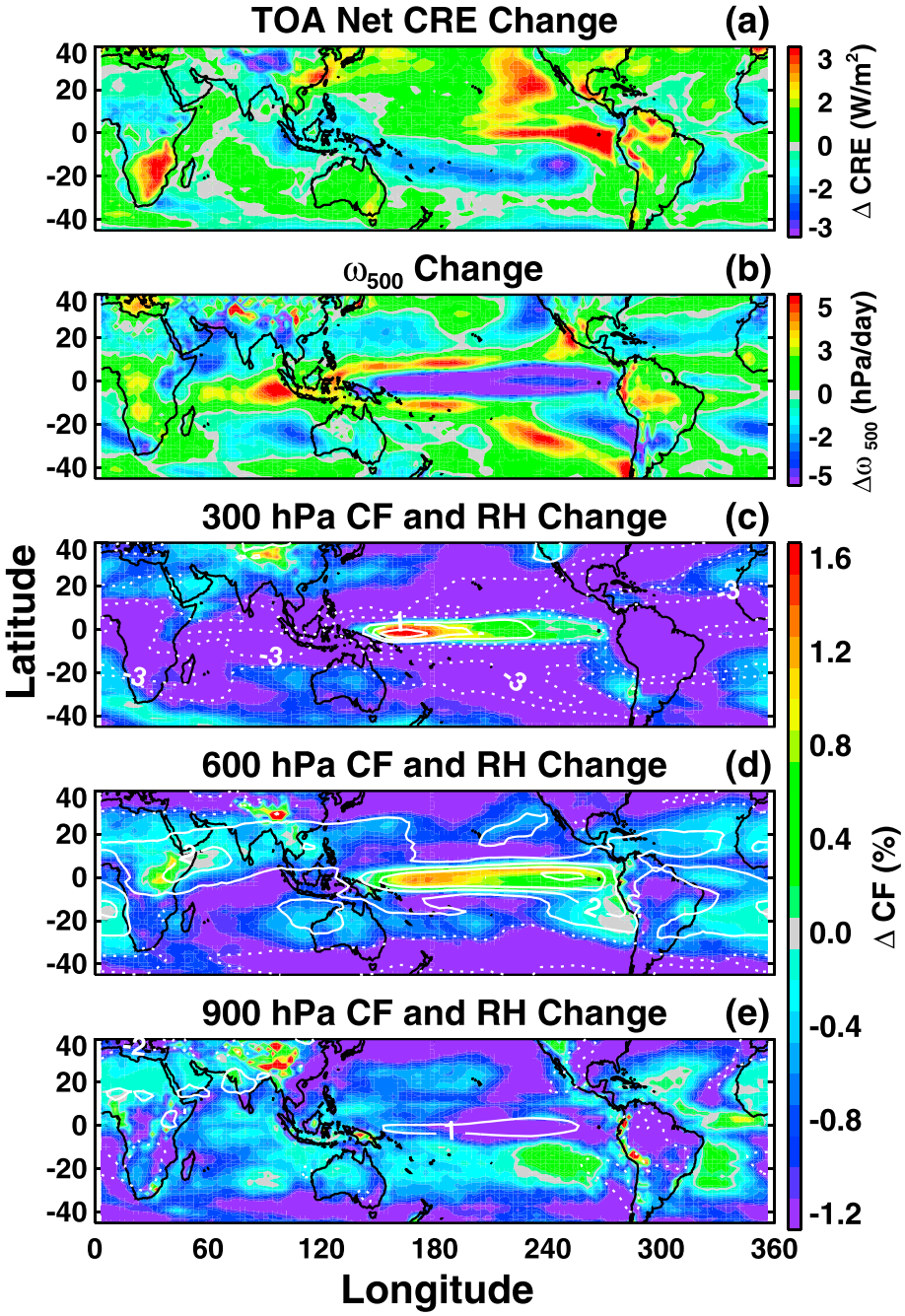

Figure 3. The spatial maps of changes in TOA net CRE, ω_{500}, cloud fraction, and relative humidity from the present day to the end of the 21st century projected in the RCP 4.5 scenario for the multimodel mean. (a) TOA net CRE, (b) vertical pressure velocity at 500 hPa, (c) 300 hPa cloud fraction (color shadings) and relative humidity (white contours), (d) 600 hPa cloud fraction (color shadings) and relative humidity (white contours), and (e) 900 hPa cloud fraction (color shadings) and relative humidity (white contours).

cloud changes (Figure 3). Partially compensating cloud fraction and relative humidity changes make relatively small zonal-mean changes within 15°–30°N/S compared to other latitudinal bands (Figure 1b).

At the TOA, a net warming effect by clouds prevails in the subtropics (Figure 1c), with a greater warming effect in the northern hemisphere, primarily over the northeast Pacific region (Figure 3a). Observational evidence of positive low cloud feedback in this region has been documented in previous studies [e.g., *Clement et al.,* 2009].

In the southern subtropics, increased low clouds over the southeast Pacific are counteracted by decreased clouds elsewhere (Figure 3), leading to a moderate net cloud warming effect in the zonal mean (Figure 1c).

In the latitude bands between 30°–40°N and 30°–45°S, increasing large-scale subsidence is found, corresponding to another two strengthening segments in the Hadley Circulation change (Figure 1a). The increase of subsidence there is indicative of the poleward expansion of the descent zone [*Lu et al.*, 2007] and the widening of the tropics [*Fu et al.*, 2006; *Seidel et al.*, 2008; *Davis and Rosenlof,* 2012]. A substantial decrease of free tropospheric cloud amount and relative humidity (Figure 1b) is associated with the enhanced subsidence, although the increased cloud warming (i.e., reduced cloud cooling; Figure 1c) there may be contributed primarily by the decrease of cloud water path driven by increased LTS and not by the poleward shift of extratropical storm tracks [*Kay et al.*, 2014].

3.3. The Importance of Weakening and Strengthening Structures of the Hadley Circulation Change

In summary, the change of the Hadley Circulation under global warming contains complex meridional structures. Although the overall weakening of the circulation over the entire tropics is simulated by the models in accordance with simple theories, zones of acceleration and deceleration alternate in latitude, accompanied by the narrowing and widening of the ascent and descent regions, respectively. Separating the weakening and strengthening segments of the Hadley Circulation change provides a clear linkage between the large-scale circulation and cloud changes. Using the maximum value of the zonal-mean stream function or velocity potential to represent the Hadley Circulation, as done conventionally, would thus obscure the connection between the Hadley Circulation and changes of clouds in different cloud regimes. Note that the zonally asymmetric components of circulation and cloud changes can be large and important but are not dealt with here.

For the multimodel mean, the changes of TOA net CRE are greater than zero everywhere within the Hadley Cell between 45°S and 40°N, despite that the longwave CREs may be negatively biased because of the cloud masking effects [*Soden et al.*, 2008; *Zelinka et al.*, 2013]. The latitudinal zones with a strengthening of ascent or descent account for about 46% of the area-weighted integral of the CRE change, compared to 54% from the latitudinal bands with a weakening of ascent or descent. It is fair to say that the weakening and strengthening segments of the Hadley Circulation change contribute nearly equally to the cloud and CRE changes at the end of the 21st century in the RCP 4.5 scenario.

4. Quantifying the Intermodel Spread in the Hadley Circulation Change and Its Relationship With CRE Change and Cloud Feedbacks

4.1. The Empirical Orthogonal Function Analysis

To quantify the magnitude of the meridionally varying structures in the Hadley Circulation change for each model, we apply an empirical orthogonal function (EOF) analysis to the 15 models' zonal-mean vertical velocity change at 500 hPa (ω_{500}) within 45°S–40°N (using the full vertical velocity profile yields similar results). In this EOF analysis, the spatial pattern of interest is the change of zonal mean ω_{500} as a function of latitude. Each model is equivalent to a "time slice" in the conventional temporal series for EOF analysis. The principal components (PCs) of the leading EOF mode represent the magnitudes of the dominant structure of the Hadley Circulation change for all models. By so doing, we can objectively determine the magnitude of the meridionally varying structures of the Hadley Circulation change for each model and avoid biases by using local indices. A similar method was used in a recent study to identify the SST warming patterns and amplitudes in a number of model simulations [*Tokinaga et al.*, 2012].

The resulting first EOF mode explains 57% of the variance across the models. The corresponding meridional structure of the first EOF mode is shown in Figure 4a. It resembles the multimodel mean ω_{500} change (Figure 1a), suggesting that the meridional structure of the Hadley Circulation change discussed in the preceding section is a dominant feature shared by all models. Combined with climatological ω_{500} (Figure 4a, dashed line), the first EOF mode of ω_{500} change clearly defines the "strengthening" and "weakening" segments of the Hadley Circulation change, marked in Figure 4a. The PCs of the first EOF mode have values between 0.026 and 2.0 (Figure 4b), 2 orders of magnitude difference among the models, suggesting a tremendous disagreement among the models in terms of dynamic response to surface warming and to forcings in the projected climate change scenario, as found in earlier studies [e.g., *Bony et al.*, 2013].

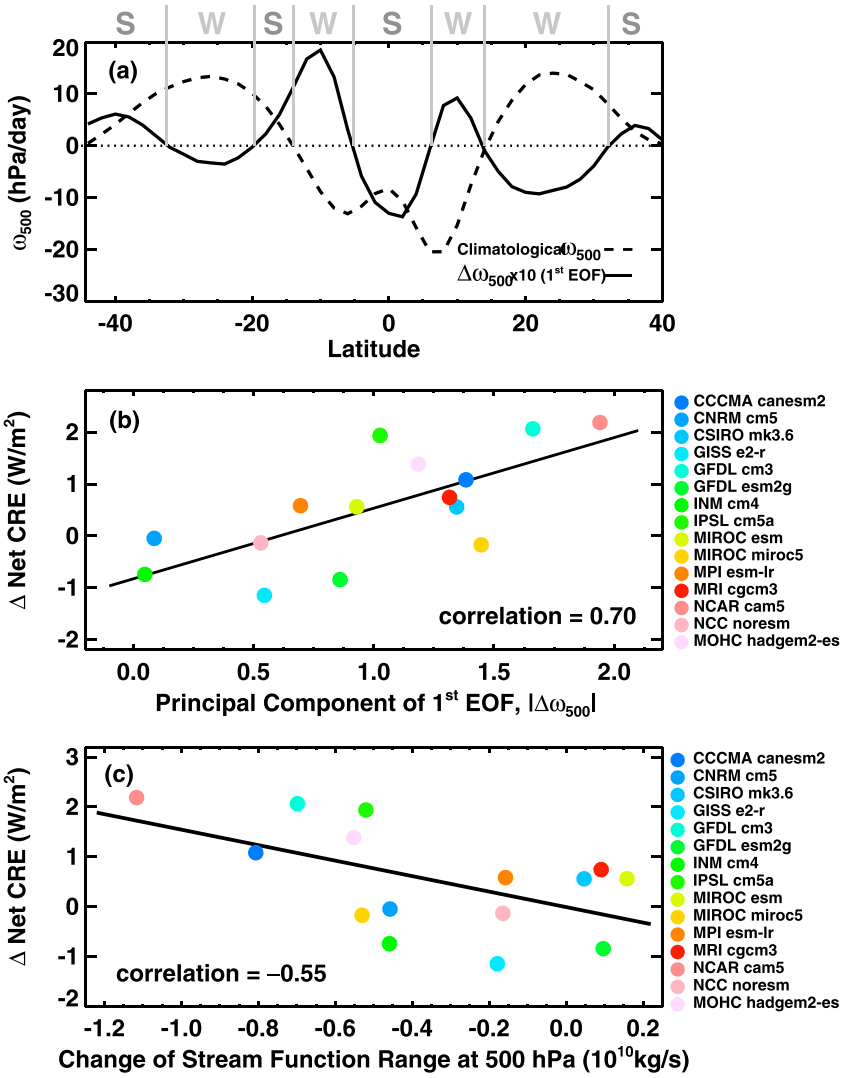

Figure 4. (a) Meridional structure of the first EOF mode of the 500 hPa vertical pressure velocity (ω_{500}) change across the 15 models superimposed with climatological ω_{500}. The amplitude of the first EOF mode is enlarged by 10 times. "S" and "W" denote the "strengthening" and "weakening" segments of the Hadley Circulation change, respectively. (b) The principal component of the first EOF mode for the Hadley Circulation change versus changes in TOA net CRE averaged between 45°S and 40°N for the 15 models. (c) The change of zonal-mean mass-weighted stream function range at 500 hPa versus changes in TOA net CRE averaged between 45°S and 40°N for the 15 CMIP5 models. The solid lines are the least squares linear fits to the data, with correlation coefficients marked.

Correlating the PCs of the first EOF mode with the changes in TOA net CREs averaged between 45°S and 40°N yields a remarkably high positive correlation, 0.70 (Figure 4b), statistically significant at 99% based on two-sided Student's *t* test.

For comparison, we compute the range of zonal-mean mass-weighted stream function at 500 hPa (ψ_{500}), as commonly used for the Hadley Circulation strength. Zonal-mean stream function is calculated by the integral of vertical pressure velocity over each latitude band between 90°S and 90°N and weighted by area [*Oort and Yienger*, 1996]. The results are the same if zonal-mean meridional wind profiles are integrated vertically for the calculation of the stream function. The strength of the Hadley Circulation is indicated by the range (maximum minus minimum) of ψ_{500}. The resulting change of the ψ_{500} range for each model is found to be negatively correlated with the averaged CRE within 45°S–40°N (Figure 4c), corroborating the co-variability between the Hadley Circulation change and the CRE change. The correlation coefficient between the change of ψ_{500} range and CRE is −0.55 (statistically significant at 95% level), somewhat lower than that between the

PCs and CREs (Figure 4b). The smaller variance of the CRE change explained by the stream function than by the PCs indicates that the meridional varying structures of the Hadley Circulation change are more meaningful for understanding the relations between the Hadley Circulation change and cloud change than broadly averaged indices such as the stream function. The PCs capture the model differences in simulating the distinct "strengthening" and "weakening" circulation regimes that are associated with different cloud types. They are found to be particularly useful to depict the complex pattern of circulation changes in a holistic and quantitative way.

4.2. Normalizing the Circulation and CRE Changes by Surface Temperature Change

One might wonder if the correlations shown in Figures 4b and 4c arise from the fact that both circulation and CRE changes would be larger in the models with larger increases in global-mean surface temperature. Indeed, the circulation and CRE changes are both strongly correlated with the global-mean surface temperature changes with the correlations at 0.61 and 0.81, respectively. A normalization by global-mean surface temperature or ECS would be a simple way to remove the model spread caused by the different temperature warming, although caveats exist because parts of the circulation and CRE changes are driven by forcings and thus not temperature dependent. Such caveats will be discussed more in detail in section 5. Here we present the ECS-normalized results and examine whether the strong correlation between the circulation and CRE changes still holds after the impact of surface warming is removed. Using global-mean surface temperature change to normalize the variables yields similar results to the ECS-normalized quantities. Only the ECS-normalized results are shown.

Figure 5 shows the spatial distributions of ECS-normalized ω_{500}, TOA net CRE, precipitation, and 300 hPa and 900 hPa cloud fraction changes per degree of warming for two model composites consisting of the top or bottom five models with the largest or smallest normalized PCs. The regions where the differences between the two model composites are statistically significant above 75% level are marked by white stipples with a white outline. All quantities discussed below refer to the normalized changes by ECS listed in Table 1.

The maps of ω_{500} change highlight the zonal asymmetry of circulation changes as the grouping is based on the zonal-mean Hadley Circulation change index, i.e., the PCs (Figures 5a and 5f). The weakening of the Walker Circulation is evident across the equatorial Indian Ocean and the Pacific Ocean in both model composites. The group with a larger change in the Hadley Circulation also exhibits a larger weakening of the Walker Circulation. The Intertropical Convergence Zone (ITCZ) and the northeast and southeast Pacific and the Atlantic Oceans stand out as the sensitive regions with statistically significantly different vertical velocity changes between the two model composites.

Accompanying the largest circulation changes, the normalized net CRE changes show increased net cloud warming over most of the 45°S to 40°N, except for some parts over South Pacific and Atlantic. The equatorial eastern Pacific, North Pacific, and Atlantic storm track regions have substantial net cloud warming effects. On the other hand, the model composite with the smallest circulation change shows enhanced net cloud cooling or less warming at the TOA (Figures 5b and 5g) over most of the domain. Note that the CRE changes shown here are relative to the present day, not relative to the preindustrial condition.

The precipitation change is closely related to the circulation change in that the increase (decrease) of upward motion over the ITCZ is associated with the increase (decrease) of precipitation, with the magnitude differences consistent with the vertical velocity changes (Figures 5c and 5h). These precipitation changes are representative of tropospheric latent heating changes associated with deep convection, closely resembling the 300 hPa cloud fraction changes over the tropics (Figures 5d and 5i).

In the boundary layer at 900 hPa (similarly at 850 hPa), the changes of cloud fraction between the two model composites are strikingly different (Figures 5e and 5j). The model composite with the largest normalized circulation changes produces a widespread reduction of low cloud fraction, while the model composite with the smallest circulation changes produces an increase of low cloud fraction over most of the domain. The differences between the two composites are statistically significant over the equatorial eastern Pacific, North Pacific and North Atlantic. As the low cloud amount is predominantly important for the TOA net CRE and cloud feedbacks, the circulation stratified differences in the low cloud fraction change suggest that the inter-model spread in cloud feedbacks is closely associated with the model differences in the large-scale circulation changes.

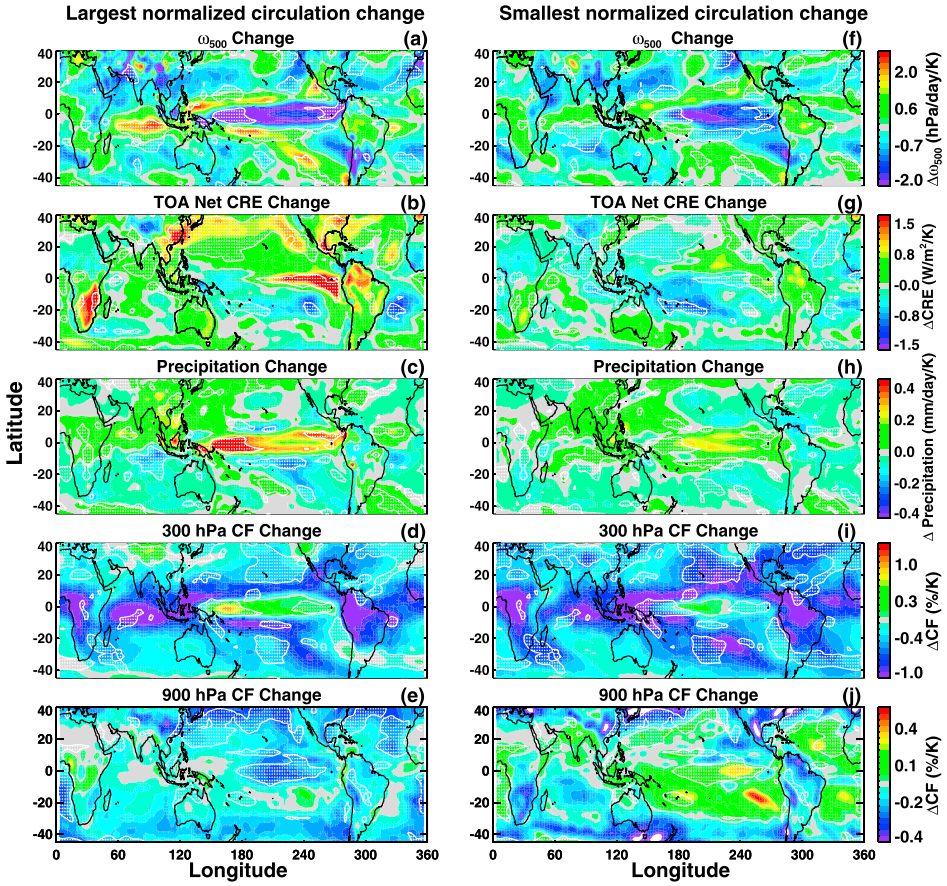

Figure 5. The model composites based on the ECS-normalized circulation changes indicated by the PCs of the first EOF. The left (right) panels correspond to the averages from the top (bottom) five models with the largest (smallest) normalized circulation changes. (a and f) ω_{500}, (b and g) TOA net CRE, (c and h) precipitation, (d and i) 300 hPa cloud fraction (CF), and (e and j) 900 hPa cloud fraction. All quantities are the ECS-normalized changes from the present day to the end of the 21st century projected in the RCP 4.5 scenario. The stippled areas with white outlines indicate that the differences between the two composites are statistically significant above the 75% level.

While the increase of high clouds with the increase of ascent over the deep convective regions are well understood, how weakened large-scale subsidence over the stratocumulus regions could cause the decrease of low clouds is less obvious. *Myers and Norris* [2013] and *Bretherton et al.* [2013] argued that the decrease of large-scale subsidence alone would raise stratocumulus cloud top and increase low cloud fraction, although observed interannual and decadal changes of low cloud fraction appear to be positively correlated with the strengthening of subsidence [*Clement et al.*, 2009]. A plausible process that could connect the weakened subsidence and reduced low cloud fraction is the enhanced drying of the boundary layer in a warmer climate [*Sherwood et al.*, 2014]. When subsidence weakens, the boundary layer deepens [*Bretherton et al.*, 2013; *Blossey et al.*, 2013], permitting more mixing between the free troposphere and the boundary layer [*Rieck et al.*, 2012; *Stevens*, 2007]. The increased mixing would lead to a greater drying of the boundary layer and a subsequent reduced low cloudiness [*Bretherton et al.*, 2013; *Sherwood et al.*, 2014].

Figure 6 explores the correlation between the boundary layer drying and large-scale circulation change for the 15 models. Taking a box over the northeast Pacific region where stratocumulus clouds dominate (15°–25°N, 115°–145°W), the same area analyzed by *Clement et al.* [2009], we calculate the relative humidity difference between 700 hPa and 850 hPa ($\Delta RH = RH_{700} - RH_{850}$), which represents the humidity gap between the free troposphere and the cloudy boundary layer (using the relative humidity difference between 700 hPa and 900 hPa yields similar results). Climatological mean ΔRH is negative in most models. Under global warming, a positive change of ΔRH from the present day indicates that the boundary layer becomes less moist compared to

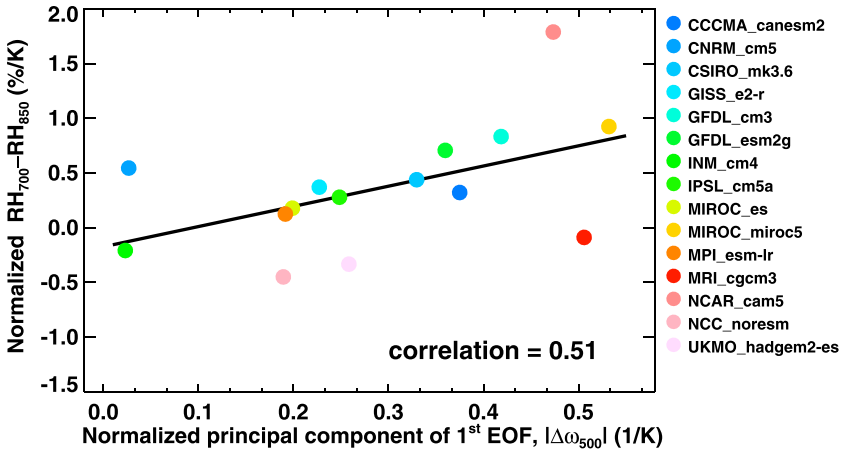

Figure 6. The ECS-normalized circulation changes versus the ECS-normalized changes of relative humidity difference between 700 hPa and 850 hPa averaged over a box (15°–25°N, 115°–145°W) in the northeast Pacific. The solid line is the least squares linear fit to the data, with correlation coefficient marked.

the free troposphere. The ECS-normalized changes of ΔRH between the end of the 21st century and the present day averaged over this box for the 15 models are found to be correlated with the normalized PCs at 0.51, statistically significant at 95% level, suggesting that the models with the larger Hadley Circulation changes (the greater PCs) tend to have a greater drying of the boundary layer (the more positive change of ΔRH), which could contribute to a greater decrease of low clouds. Note that our index of "boundary layer drying," ΔRH, is different from the "convective mixing" index used in *Sherwood et al.* [2014] in that their convective mixing index is defined over deep convective regions while our "boundary layer drying" index is defined over the subtropical subsidence regions, and the changes of ΔRH under global warming are of interest here.

Averaging the normalized TOA CRE changes zonally, the two model composites stratified by the normalized circulation changes exhibit outstanding differences (Figure 7). The composite mean for the top five models with the largest normalized circulation changes yields positive net CRE changes (increased cloud warming) at almost all latitudes within the Hadley cell, while the composite mean for the bottom five models with the smallest circulation changes yields negative net CRE changes at all the latitudes except over the limited zones poleward of 30°S/N. The TOA net CRE changes are dominated by the shortwave CRE changes, with the longwave CRE changes counteracting the shortwave effects. Note that the longwave CREs are negatively biased due to the cloud masking effects. For the model composite of the largest normalized circulation changes (Figure 7a, red curve), the northern hemispheric subtropics show a noticeably higher positive net CRE change than the southern hemispheric subtropics, consistent with the greater reduction of the boundary layer clouds at 900 hPa in the north than in the south shown in Figure 5e. *Soden and Held* [2006] showed that the model differences in the CRE changes are well correlated with the "true" cloud feedbacks so that it is reasonable to expect that the two model composites stratified by the circulation changes have significantly different cloud feedbacks.

Figure 8 further examines the correlation of normalized circulation and CRE changes for all 15 models. The normalized PCs are correlated with normalized TOA net, shortwave, and longwave CRE changes averaged over 45°S and 40°N at correlation coefficients of 0.39, 0.47 (Figures 8a and 8b), and −0.41 (not shown), respectively. The larger circulation changes correspond to stronger net cloud warming (reduced cloud cooling) effects. The model differences in circulation changes explain about 15% (22%) of the intermodel spread in the net (shortwave) CRE changes per degree of equilibrium surface temperature change. The normalized net (shortwave) CRE change is correlated with ECS at 0.77 (0.54) (Figures 8c and 8d), while there is very little correlation between the longwave CRE change and ECS.

5. Discussions

There are a few caveats worth mentioning. First, the CRE changes include the cloud masking effects [*Soden et al.*, 2004] and rapid cloud adjustments to forcings, not dependent on surface warming [*Zelinka et al.*, 2013].

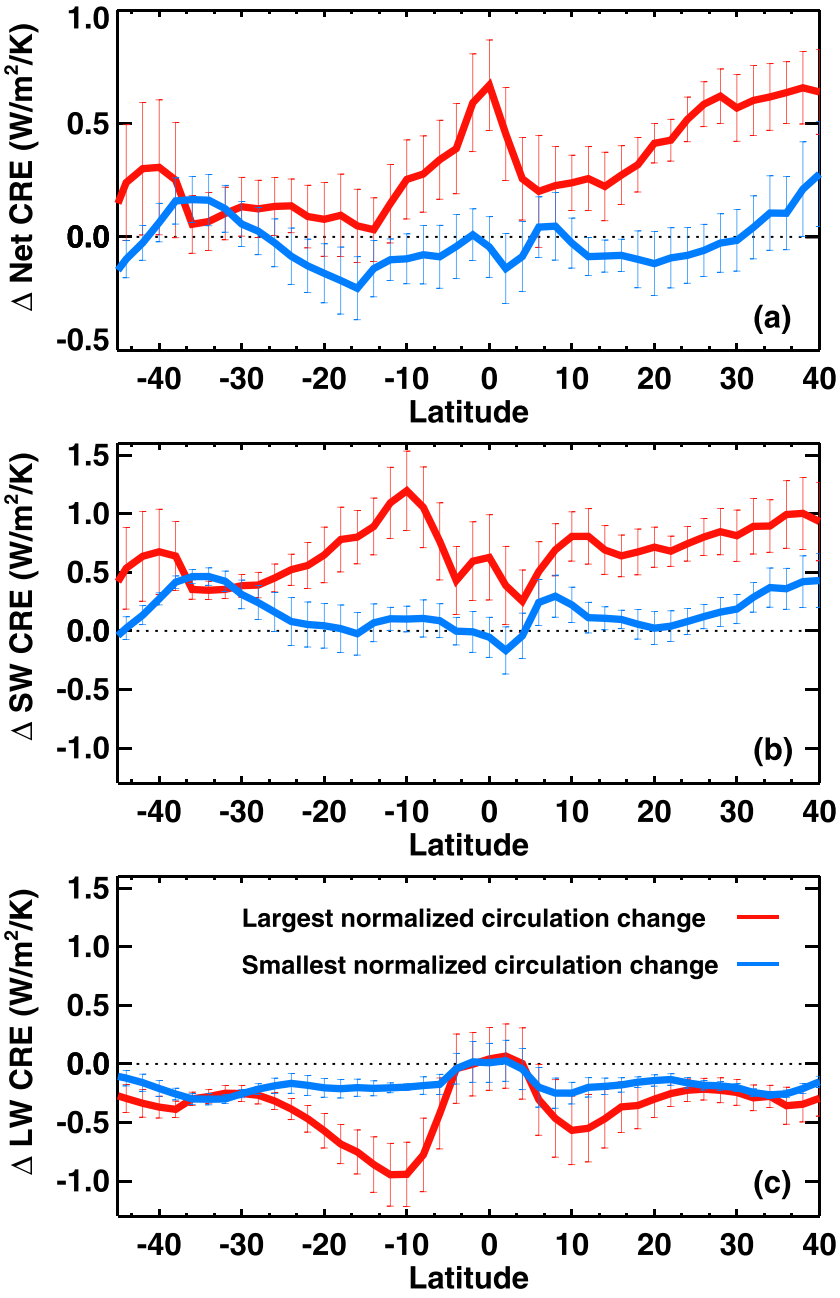

Figure 7. The model composites of the area-weighted zonal-mean TOA CRE changes. Red (blue) curves correspond to the averages from the top (bottom) five models with the largest (smallest) normalized circulation changes. Error bars indicate the standard errors of the normalized CRE changes for each model composite. (a) net and (b) shortwave and (c) longwave CRE changes normalized by ECS from the present day to the end of the 21st century projected in the RCP 4.5 scenario.

The cloud masking effects tend to make the CRE-derived cloud feedbacks negatively biased compared to the cloud feedbacks calculated from cloud radiative kernels [*Zelinka et al.*, 2013] or adjustment of cloud forcings using standard radiative kernels [*Soden et al.*, 2008; *Shell et al.*, 2008]. The cloud masking effects produce a larger bias in longwave CRE than in shortwave CRE. The negative biases tend to be systematic across the models [*Soden et al.*, 2008; *Zelinka et al.*, 2013] so that the intermodel spread in normalized CRE changes bears some resemblance to the intermodel spread in kernel-derived cloud feedbacks, especially for the shortwave components.

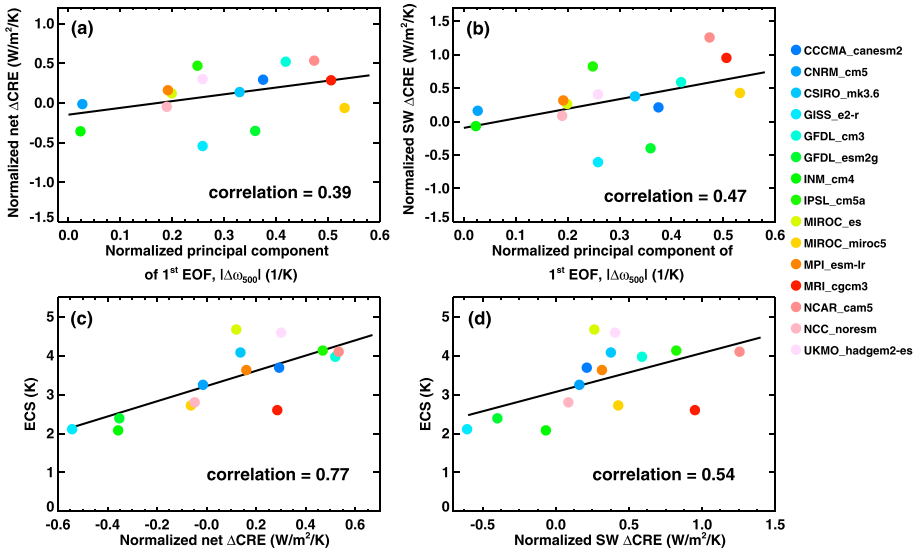

Figure 8. The ECS-normalized circulation changes versus the ECS-normalized (a) TOA net and (b) shortwave CRE changes, and the ECS-normalized (c) TOA net and (d) shortwave CRE changes versus ECS. The solid lines are the least squares linear fits to the data, with correlation coefficients marked.

Second, we recognize that the circulation and CRE changes from the historical runs to the RCP 4.5 scenario are not simply scaled by the degrees of surface warming. Various forcing agents, such as greenhouse gases, aerosols, stratospheric ozone, and land surface conditions evolve with time. The magnitudes of adjusted forcings at 2095 under the RCP 4.5 differ by as much as $2\,W\,m^{-2}$ in the 15 models [*Meinshausen et al.*, 2011; *Forster et al.*, 2013]. Model-simulated circulation and cloud changes depend on the magnitude and nature of the forcings. *Forster et al.* [2013] showed that the intermodel spread of surface temperature change at 2095 is primarily driven by climate feedback differences, but the adjusted forcing differences also play a role. For example, the aerosol indirect effects on clouds, as an unconstrained forcing in the models, could create large intermodel spread in circulation and cloud changes. Moreover, rapid cloud adjustment to CO_2 forcings exhibits considerable spread among the models. It is difficult to systematically remove the impact of rapid cloud adjustments on CRE changes without idealized model experiments. Accurate quantification of cloud feedbacks and their relation to dynamic response would require analyzing additional model simulations such as the abrupt quadrupling of CO_2 runs (abrupt4 × CO_2) combined with perturbed SST runs ("amip + 4 K") and corresponding control runs [*Taylor et al.*, 2012], and utilizing radiative kernels for calculations of cloud feedbacks [e.g., *Shell et al.*, 2008; *Soden et al.*, 2008; *Zelinka et al.*, 2013].

Third, different SST patterns in the coupled simulations may produce different circulation changes [*Tokinaga et al.*, 2012; *Ma et al.*, 2012; *Ma and Xie*, 2013] even when the averaged surface temperature warming is the same. Hence, the simple normalization by global-mean surface temperature change has inherent limitations.

Nevertheless, our analysis offers a new perspective to understand the intermodel spread in cloud response and climate sensitivity. The correlation between the intermodel spreads in circulation and CRE changes highlights the close coupling between large-scale circulation and clouds. The circulation differences could drive part of the cloud differences, while the cloud differences may feedback onto the global and regional energetics and cause circulation differences. Many previous studies show that the cloud parameterization differences are the primary source of the discrepancy for cloud simulations [*Medeiros et al.*, 2008; *Medeiros and Stevens*, 2011; *Su et al.*, 2013], while this analysis shows that the cloud differences bear the signature of circulation differences and vice versa. Thus, the uncertainty of cloud feedbacks (and climate sensitivity) lies in the intimate coupling between large-scale circulation and clouds. It is possible that both circulation and cloud change differences are fundamentally driven by the unresolved convective and cloud processes parameterized differently in climate models [*Stevens and Bony*, 2013]. As dynamic and thermodynamic factors are coupled together, it is difficult to isolate the cause and effect based on the simple correlations. More in-depth analyses including cleverly designed model sensitivity experiments are needed to fully understand the interactions between large-scale circulation and clouds.

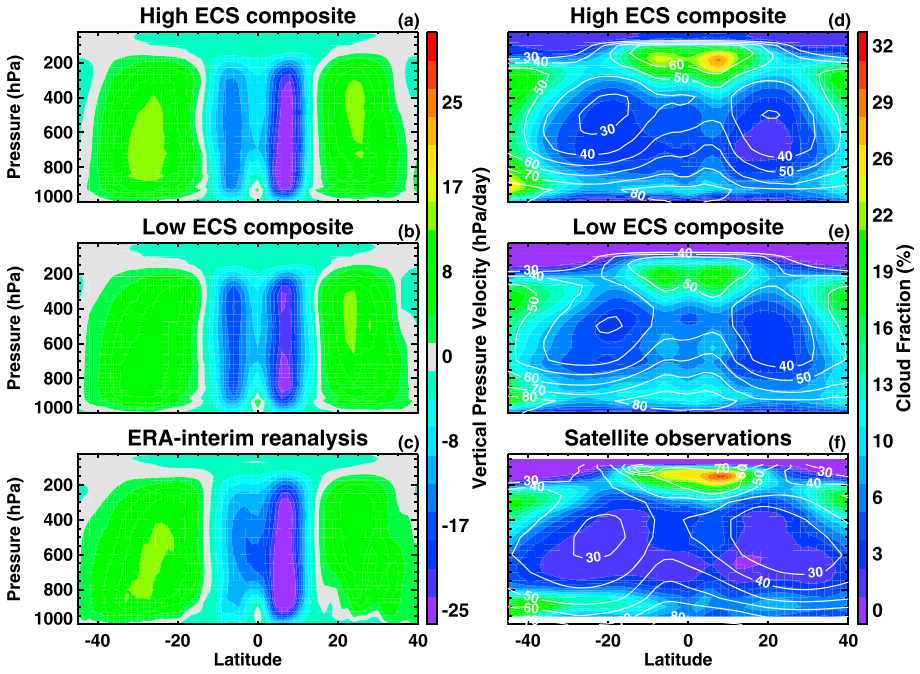

Figure 9. Present-day climatological zonal-mean ω, cloud fraction, and relative humidity for the high- and low-sensitivity model composites, compared to the observations. ω in color shadings for the (a) high- and (b) low-sensitivity model composites and the (c) ERA-interim reanalysis. Cloud fraction in color shadings and relative humidity in contours for the (d) high- and (e) low-sensitivity model composites and the (f) A-Train satellite observations. The joint cloud fraction retrievals from CloudSat/CALIPSO and the combined relative humidity retrievals from AIRS/MLS are used for observations.

6. New Model Performance Metrics Representing the Close Linkage Between the Hadley Circulation and Clouds

Recent studies showed that model simulations of certain parameters and processes in present-day climate are correlated with models' ECSs so that model performances of present-day climate can provide a constraint on ECSs [*Fasullo and Trenberth*, 2012; *Sherwood et al.*, 2014]. As large-scale circulation is closely coupled with cloud response, constraining model representation of large-scale circulation and its variations is therefore important for reducing the uncertainties of climate projections.

We have shown that spatially varying cloud changes are associated with complex structured circulation changes over all the latitudes of the Hadley cell. Thus, it is highly desirable to devise new model performance metrics that capture the entire spatial variations of clouds (and/or relative humidity) within the Hadley cell boundaries. Vertical velocity is a model-derived quantity in the reanalysis, and different reanalysis data sets produce quite different vertical motions for which error estimation is difficult to perform. While the vertical velocity field itself does not provide a ready independent observational constraint, new metrics using relative humidity and cloud profiles can be formulated to indicate model performance in representing the large-scale circulation.

The connection between the meridional structure of the Hadley Circulation and the spatial distributions of clouds and relative humidity in the present-day climate is illustrated in Figure 9. Comparing the high- and low-sensitivity model composites of present-day climatological zonal-mean vertical velocity with their respective cloud fraction and relative humidity profiles, we find that the high-sensitivity model composite has higher relative humidity and more cirrus clouds in the tropical upper troposphere along with drier and less cloudy subtropics, consistent with stronger maximum tropical ascent and subtropical descent in the zonal-mean vertical pressure velocity. The differences between the two model composites in cloud and relative humidity profiles are consistent with their circulation differences. Hence, the spatial distributions of cloud and relative humidity can serve as proxies of large-scale circulation, which is difficult to observe directly from space.

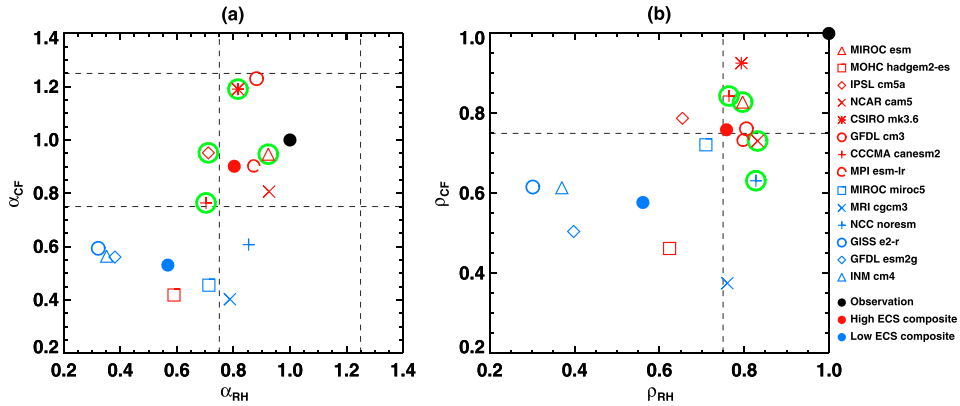

Figure 10. Model performance metrics that capture the spatial variations of zonal-mean cloud fraction and relative humidity associated with the Hadley Circulation. (a) Regression slopes (α_{CF}) of model zonal-mean cloud fraction profiles onto the joint CloudSat/CALIPSO cloud fraction versus the regression slopes (α_{RH}) of model zonal-mean relative humidity profiles onto the combined AIRS/MLS relative humidity between the surface and 100 hPa from 45°S to 40°N. (b) Similar to Figure 10a, except for the spatial correlations between the model and observed cloud fraction (ρ_{CF}) and relative humidity (ρ_{RH}) profiles. The dashed lines mark the boundaries of the "best estimates" based on observational data uncertainty of 25%. The red and blue colors denote high- and low-sensitivity models, respectively, with the red and blue solid circles corresponding to the ensemble composites for the high- and low-sensitivity models, respectively. The solid black circles denote observations. Only 14 models are shown because CNRM cm5 does not provide cloud fraction profiles in the historical run at the CMIP5 archive. The green circles mark the top four models that have the highest regression or correlation in terms of zonal-mean vertical pressure velocity with the ERA-interim reanalysis.

Furthermore, comparing the model simulations against the ERA-interim reanalysis and A-Train satellite observations, we find that the high-sensitivity composites agree better with the observations than the low-sensitivity composites in terms of the maximum ascent/descent and the meridional and vertical variations of cloud fraction and relative humidity. The differences in cloud fraction and relative humidity between the high- and low-sensitivity model composites are reminiscent of the changes under global warming (Figure 1b). Additionally, the contrasts between the tropical upper troposphere and subtropical free troposphere are even greater in the observations than those in either high- or low-sensitivity model composites. These results are consistent with previous studies that suggested the high-sensitivity models are likely more "realistic" than the low-sensitivity models [*Fasullo and Trenberth*, 2012; *Klein et al.*, 2013; *Sherwood et al.*, 2014]. Departing from previous studies that focused on local indices, we emphasize here that the complete meridional and vertical structures of cloud fraction and relative humidity are important for constraints of climate sensitivity because of their close association with the large-scale circulation.

To quantify the models' performance in representing the coherent spatial variations of cloud fraction and relative humidity associated with the Hadley Circulation, we compute the regression slopes of the model zonal-mean cloud fraction and relative humidity (α_{CF} and α_{RH}) onto the observed profiles as well as the spatial correlations between the model and observed profiles (ρ_{CF} and ρ_{RH}) between the surface and 100 hPa within 45°S to 40°N (Figure 10). These metrics would yield a value of 1 when the models and observations match perfectly (Figure 10, solid black circles). Although cloud fraction and relative humidity are two highly correlated quantities, the observed cloud fraction and relative humidity measurements are taken from independent instruments and thus can serve as two observational constraints.

Based on these "global" metrics germane to the entire Hadley Circulation, we find that the models that are closer to the observations tend to have ECS higher than the multimodel mean (labeled in red), while the low-sensitivity models (labeled in blue) are generally farther away from the observations. The high- and low-sensitivity model composites are clearly separated in terms of the deviation from the observations with the high-sensitivity composite being much closer. Because of the strong correlation between cloud fraction and relative humidity, the regression slopes and spatial correlations are distributed approximately diagonally: low (high) α_{CF} and ρ_{CF} are usually associated with low (high) α_{RH} and ρ_{RH}. Considering the observational data uncertainty of about 25% for cloud fraction and relative humidity, we may crudely define the "best estimates"

as those models with α_{CF} and α_{RH} between 0.75 and 1.25, or with ρ_{CF} and ρ_{RH} between 0.75 and 1.0. With these cutoff values, we find that only five high-sensitivity models plus the high-sensitivity composite fit into the area of "best estimates." We caution that the limited model samples examined here do not necessarily provide robust statistics of ECS. However, the tendency of better performing models to have higher ECS is in general agreement with earlier studies [*Tung et al.*, 2008; *Fasullo and Trenberth*, 2012; *Klein et al.*, 2013; *Sherwood et al.*, 2014].

Similar regressions and correlations are conducted for the model-simulated zonal-mean vertical pressure velocity profiles against the ERA-interim reanalysis data. Only the top four models with the highest coefficients ranging from 0.91 to 1.09 for regressions and 0.95 to 0.97 for correlations are marked in green circles in Figure 10. Note that the coefficient differences between the models are rather small and no objective uncertainty estimates for the vertical velocity are available. Roughly speaking, the top four models having the highest regressions or correlations with the ERA-interim reanalysis vertical pressure velocity generally reproduce well the observed cloud fraction and relative humidity profiles. This confirms that the meridional and vertical structures of clouds and relative humidity can be proxies of the Hadley Circulation.

7. Conclusions

This study establishes the close linkage between the meridional structures of the Hadley Circulation change and the cloud response under global warming. The change of the Hadley Circulation exhibits latitudinally alternating strengthening and weakening structures with each segment physically consistent with the cloud and CRE changes. The strengthening and weakening segments of the Hadley Circulation contribute about equally to the total CRE changes within the boundaries of the Hadley Cell on the multimodel mean. Our study underscores the need to better understand large-scale circulation changes at scales smaller than averages over the entire Hadley cell for the contribution of circulation to the cloud response and climate sensitivity.

The dominant mode of the structures in the Hadley Circulation change, derived from the EOF analysis across the models, resembles the multimodel mean. When normalized by ECS, the magnitudes of this leading EOF mode differ by approximately 18 times across the 15 climate models analyzed, highlighting large intermodel spread in the dynamic response in the RCP 4.5 scenario. The model spread in the TOA CRE change is highly correlated with the model spread in the first EOF mode. The intermodel differences in the circulation change account for about 15% (22%) of the intermodel spread in the TOA net (shortwave) CRE change in the RCP 4.5 scenario.

Normalizing the circulation and CRE changes by ECS, we show that the models having the largest circulation changes would produce greater positive CREs and stronger positive cloud feedbacks. The positive CRE changes are primarily caused by the reduction of clouds over the subtropical stratocumulus regions and near storm tracks. The drying of the boundary layer associated with the weakened subsidence is a plausible process that leads to the decrease of low clouds. Across the models, the intermodel differences in the extent of the boundary layer drying are correlated with the magnitudes of the Hadley Circulation change. The close linkage between large-scale circulation and cloud response points to the need of understanding the uncertainty of cloud feedbacks through the coupling between the circulation and clouds and the importance of constraining models' representation of moist dynamics with observations for improving climate change predictions.

We recognize that the inference of cloud feedback based on the CREs from the RCP 4.5 experiments could have inherent biases associated with the cloud masking effects and rapid cloud adjustments. Different aerosol effects may be also responsible for the intermodel spread in cloud responses. Future work is needed to quantify cloud feedbacks and their relations with circulation changes through the use of cloud or standard radiative kernel technique [e.g., *Zelinka et al.*, 2013; *Soden et al.*, 2008; *Shell et al.*, 2008] and idealized model experiments with simplified forcings in coupled or uncoupled scenarios.

Lastly, the new model performance metrics that emphasize the entire spatial variations of cloud fraction and relative humidity associated with the Hadley Circulation show that the models that perform better by these measures tend to have higher ECS. These models also produce stronger Hadley Circulation in general. Consistent with this, composites over the high-sensitivity models perform substantially better by these measures than those over the low-sensitivity models. Although better performance in current climate is not

necessarily an indicator of a better projection of future climate, these new metrics are for climate variables closely associated with circulation and energy budget changes under global warming. Any reasonable weighting of the multimodel ensemble by these metrics would yield an estimate of ECS higher than the multimodel mean.

Acknowledgments

We are thankful to Jay Mace, Eric J. Fetzer, and William G. Read for helpful discussions of data quality. Discussions with Kevin Bowman, Duane Waliser, and Michael Gunson are appreciated. This paper is greatly improved owing to the detailed comments and constructive suggestions by Mark Zelinka and two other reviewers. We acknowledge the World Climate Research Programme's Working Group on Coupled Modelling, which is responsible for CMIP. We thank the climate modeling groups listed in Table 1 for producing and making available their model output. The U.S. Department of Energy (DOE) Program for Climate Model Diagnosis and Intercomparison provides coordinating support and led development of software infrastructure in partnership with the Global Organization for Earth System Science Portals. The A-Train satellite data are available at NASA Distributed Active Archive Centers (DAAC). H.S., J.H.J., C.Z., and J.T.S. acknowledge funding support from NASA NEWS, COUND, and AST programs and Aura MLS and CloudSat projects. J.D.N. was supported by NOAA NA11OAR4310099 and NSF AGS-1102838. Y.L.Y. was supported by UHOUST.130027 subcontract from the University of Houston. This work was performed at Jet Propulsion Laboratory, California Institute of Technology, under contract with NASA.

References

Andrews, T., J. M. Gregory, M. J. Webb, and K. E. Taylor (2012), Forcing, feedbacks and climate sensitivity in CMIP5 coupled atmosphere-ocean climate models, *Geophys. Res. Lett.*, *39*, L09712, doi:10.1029/2012GL051607.

Blossey, P. N., C. S. Bretherton, M. Zhang, A. Cheng, S. Endo, T. Heus, Y. Liu, A. P. Lock, S. R. de Roode, and K.-M. Xu (2013), Marine low cloud sensitivity to an idealized climate change: The CGILS LES intercomparison, *J. Adv. Model. Earth Syst.*, *5*, 234–258, doi:10.1002/jame.20025.

Bodas-Salcedo, A., et al (2011), COSP: Satellite simulation software for model assessment, *Bull. Am. Meteorol. Soc.*, *92*, 1023–1043, doi:10.1175/2011BAMS2856.1.

Bony, S., and J.-L. Dufresne (2005), Marine boundary layer clouds at the heart of tropical cloud feedback uncertainties in climate models, *Geophys. Res. Lett.*, *32*, L20806, doi:10.1029/2005GL023851.

Bony, S., J.-L. Dufresne, H. Le Treut, J.-J. Morcrette, and C. Senior (2004), On dynamic and thermodynamic components of cloud changes, *Clim. Dyn.*, *22*, 71–86.

Bony, S., G. Bellon, D. Klocke, S. Sherwood, S. Fermepin, and S. Denvil (2013), Robust direct effect of carbon dioxide on tropical circulation and regional precipitation, *Nat. Geosci.*, *6*, 447–451, doi:10.1038/ngeo1799.

Bretherton, C. S., P. N. Blossey, and C. R. Jones (2013), Mechanisms of marine low cloud sensitivity to idealized climate perturbations: A single-LES exploration extending the CGILS cases, *J. Adv. Model. Earth Syst.*, *5*, 316–337, doi:10.1002/jame.20019.

Cess, R. D., et al. (1989), Interpretation of cloud-climate feedback as produced by 14 atmospheric general circulation models, *Science*, *245*, 513–515.

Chou, C., and J. D. Neelin (2004), Mechanisms of global warming impacts on regional tropical precipitation, *J. Clim.*, *17*, 2688–2701.

Clement, A. C., R. Burgman, and J. R. Norris (2009), Observational and model evidence for positive low-level cloud feedback, *Science*, *325*, 460, doi:10.1126/science.1171255.

Davis, S. M., and K. H. Rosenlof (2012), A multidiagnostic intercomparison of tropical-width time series using reanalyses and satellite observations, *J. Clim.*, *25*, 1061–1078.

Fasullo, J. T., and K. E. Trenberth (2012), A less cloudy future: The role of subtropical subsidence in climate sensitivity, *Science*, *338*, 792–794, doi:10.1126/science.1227465.

Forster, P. M., T. Andrews, P. Good, J. M. Gregory, L. S. Jackson, and M. Zelinka (2013), Evaluating adjusted forcing and model spread for historical and future scenarios in the CMIP5 generation of climate models, *J. Geophys. Res. Atmos.*, *118*, 1139–1150, doi:10.1002/jgrd.50174.

Frierson, D. M. W., and Y.-T. Hwang (2012), Extratropical influence on ITCZ shifts in slab ocean simulations of global warming, *J. Clim.*, *25*, 720–733.

Fu, Q., C. M. Johanson, J. M. Wallace, and T. Reichler (2006), Enhanced mid-latitude tropospheric warming in satellite measurements, *Science*, *312*, 1179.

Hartmann, D. L., and K. Larson (2002), An important constraint on tropical cloud-climate feedback, *Geophys. Res. Lett.*, *29*(20), 1951, doi:10.1029/2002GL015835.

Hartmann, D. L., and M. L. Michelsen (1993), Large-scale effects on the regulation of tropical sea surface temperature, *J. Clim.*, *6*, 2049–2062.

Held, I. M., and B. J. Soden (2006), Robust responses of the hydrological cycle to global warming, *J. Clim.*, *19*, 5686–5699.

Hwang, Y.-T., and D. M. W. Frierson (2013), Link between the double-Intertropical Convergence Zone problem and cloud bias over Southern Ocean, *Proc. Natl. Acad. Sci. U.S.A.*, *110*, 4935–4940, doi:10.1073/pnas.1213302110.

Jiang, J. H., et al. (2012), Evaluation of cloud and water vapor simulations in IPCC AR5 climate models using NASA "A-Train" satellite observations, *J. Geophys. Res.*, *117*, D14105, doi:10.1029/2011JD017237.

Kay, J. E., B. Medeiros, Y.-T. Hwang, A. Gettelman, J. Perket, and M. G. Flanner (2014), Processes controlling Southern Ocean shortwave climate feedbacks in CESM, *Geophys. Res. Lett*, *41*, 616–622, doi:10.1002/2013GL058315.

Klein, S. A., Y. Zhang, M. D. Zelinka, R. N. Pincus, J. Boyle, and P. J. Gleckler (2013), Are climate model simulations of clouds improving? An evaluation using the ISCCP simulator, *J. Geophys. Res. Atmos.*, *18*, 1329–1342, doi:10.1002/jgrd.50141.

Knutson, T. R., and S. Manabe (1995), Time-mean response over the tropical Pacific to increase CO_2 in a coupled ocean–atmosphere model, *J. Clim.*, *8*, 2181–2199.

Loeb, N. G., D. A. Rutan, S. Kato, and W. Wang (2014), Observing interannual variations in Hadley Circulation atmospheric diabatic heating and circulation strength, *J. Clim.*, doi:10.1175/JCLI-D-13-00656.1.

Lu, J., G. A. Vecchi, and T. Reichler (2007), Expansion of the Hadley cell under global warming, *Geophys. Res. Lett.*, *34*, L06805, doi:10.1029/2006GL028443.

Ma, J., and S.-P. Xie (2013), Regional patterns of sea surface temperature change: A source of uncertainty in future projections of precipitation and atmospheric circulation, *J. Clim.*, *26*(8), 2482–2501, doi:10.1175/JCLI-D-12-00283.1.

Ma, J., S.-P. Xie, and Y. Kosaka (2012), Mechanisms for tropical tropospheric circulation change, *J. Clim.*, *25*, 2979–2994, doi:10.1175/JCLI-D-11-00048.1.

Mace, G. G., Q. Zhang, M. Vaughan, R. Marchand, G. Stephens, C. Trepte, and D. Winker (2009), A description of hydrometeor layer occurrence statistics derived from the first year of merged CloudSat and CALIPSO data, *J. Geophys. Res.*, *114*, D00A26, doi:10.1029/2007JD009755.

Medeiros, B., and B. Stevens (2011), Revealing differences in GCM representations of low clouds, *Clim. Dyn.*, 385–399, doi:10.1007/s00382-009-0694-5.

Medeiros, B., B. Stevens, I. M. Held, M. Zhao, D. L. Williamson, J. G. Olson, and C. S. Bretherton (2008), Aquaplanets, climate sensitivity, and low clouds, *J. Clim.*, 4974–4991, doi:10.1175/2008JCLI1995.1.

Meinshausen, M., et al. (2011), The RCP greenhouse gas concentrations and their Extension from 1765 to 2300, *Clim. Change* (Special Issue), *109*, 213–241, doi:10.1007/s10584-011-0156-z.

Mitas, C. M., and A. Clement (2005), Has the Hadley cell been strengthening in recent decades?, *Geophys. Res. Lett.*, *32*, L03809, doi:10.1029/2004GL021765.

Myers, T. A., and J. R. Norris (2013), Observational evidence that enhanced free-tropospheric subsidence reduces marine boundary layer cloudiness, *J. Clim.*, *26*, 7507–7524, doi:10.1175/JCLI-D-12-00736.1.

Neelin, J. D., C. Chou, and H. Su (2003), Tropical drought regions in global warming and El Nino teleconnections, *Geophys. Res. Lett.*, *30*(24), 2275, doi:10.1029/2003GL018625.
Nguyen, H., B. Timbal, A. Evans, C. Lucas, and I. Smith (2012), The Hadley circulation in reanalyses: Climatology, variability and change, *J. Clim.*, *26*, 3357–3376, doi:10.1175/JCLI-D-12-00224.1.
Olsen, E. T., E. Manning, and S. Licata (2013), AIRS/AMSU/HSB Version 6 Data Release User Guide, Report, 67 pp., Jet Propul. Lab., Pasadena, Calif. [Available at http://disc.sci.gsfc.nasa.gov/AIRS/documentation/v6_docs/v6_docs_list.shtml#General_Documents.]
Oort, A. H., and J. J. Yienger (1996), Observed interannual variability in the Hadley circulation and its connection to ENSO, *J. Clim.*, *9*(11), 2751–2767.
Quan, X. W., H. F. Diaz, and M. P. Hoerling (2004), Change in the tropical Hadley cell since 1950, in *The Hadley Circulation: Present, Past and Future, Advances in Global Change Research*, edited by H. F. Diaz and R. S. Bradley, vol. 21, pp. 85–120, Cambridge Univ. Press, New York.
Read, W. G., et al. (2007), Aura Microwave Limb Sounder upper tropospheric and lower stratospheric H_2O and relative humidity with respect to ice validation, *J. Geophys. Res.*, *112*, D24S35, doi:10.1029/2007JD008752.
Richter, I., and S.-P. Xie (2008), Muted precipitation increase in global warming simulations: A surface evaporation perspective, *J. Geophys. Res.*, *113*, D24118, doi:10.1029/2008JD010561.
Rieck, M., L. Nuijens, and B. Stevens (2012), Marine boundary-layer cloud feedbacks in a constant relative humidity atmosphere, *J. Atmos. Sci.*, *69*, 2538–2550.
Soden, B. J., and I. M. Held (2006), An assessment of climate feedbacks in coupled ocean-atmosphere models, *J. Clim.*, *19*, 3354–3360.
Soden, B. J., A. J. Broccoli, and R. S. Hemler (2004), On the use of cloud forcing to estimate cloud feedback, *J. Clim.*, *17*, 3661–3665.
Soden, B. J., I. M. Held, R. Colman, K. M. Shell, J. T. Kiehl, and C. A. Shields (2008), Quantifying climate feedbacks using radiative kernels, *J. Clim.*, *21*, 3504–3520.
Seidel, D. J., Q. Fu, W. J. Randel, and T. J. Reichler (2008), Widening of the tropical belt in a changing climate, *Nat. Geosci.*, *1*, 21–24.
Shell, K. M., J. T. Kiehl, and C. A. Shields (2008), Using the radiative kernel technique to calculate climate feedbacks in NCAR's Community Atmospheric Model, *J. Clim.*, *21*, 2269–2282.
Sherwood, S. C., S. Bony, and J.-L. Dufresne (2014), Spread in model climate sensitivity traced to atmospheric convective mixing, *Nature*, *505*, 37–42, doi:10.1038/nature12829.
Shindell, D. T., et al. (2013), Radiative forcing in the ACCMIP historical and future climate simulations, *Atmos. Chem. Phys.*, *13*, 2939–2974, doi:10.5194/acp-13-2939-2013.
Stephens, G. L. (2005), Cloud feedbacks in the climate system: A critical review, *J. Clim.*, *18-2*, 237–273.
Stephens, G. L., and T. D. Ellis (2008), Controls of global-mean precipitation increases in global warming GCM experiments, *J. Clim.*, *21*, 6141–6155.
Stephens, G. L., J. F. Li, M. Wild, C. A. Clayson, N. Loeb, S. Kato, T. L'Ecuyer, P. W. Stackhouse Jr., M. Lebsock, and T. Andrews (2012), An update on Earth's energy balance in light of the latest global observations, *Nat. Geosci.*, *5*, 691–696, doi:10.1038/ngeo1580.
Stevens, B. (2007), On the growth of layers of nonprecipitating cumulus convection, *J. Atmos. Sci.*, *64*, 2916–2931.
Stevens, B., and S. Bony (2013), What are climate models missing?, *Science*, *340*(6136), 1053–1054, doi:10.1126/science.1237554.
Su, H., J. H. Jiang, D. G. Vane, and G. L. Stephens (2008), Observed vertical structure of tropical oceanic clouds sorted in large-scale regimes, *Geophys. Res. Lett.*, *35*, L24704, doi:10.1029/2008GL035888.
Su, H., et al. (2013), Diagnosis of regime-dependent cloud simulation errors in CMIP5 models using "A-Train" satellite observations and reanalysis data, *J. Geophys. Res. Atmos*, *118*, 2762–2780, doi:10.1029/2012JD018575.
Tanaka, H. L., et al. (2004), Trend and interannual variability of Walker, monsoon and Hadley circulations defined by velocity potential in the upper troposphere, *Tellus*, *56*, 250–269.
Taylor, K. E., R. J. Stouffer, and G. A. Meehl (2012), An overview of CMIP5 and the experiment design, *Bull. Am. Meteorol. Soc.*, *93*, 485–498, doi:10.1175/BAMS-D-11-00094.1.
Tokinaga, H., S.-P. Xie, C. Deser, Y. Kosaka, and Y. M. Okumura (2012), Slowdown of the Walker circulation driven by tropical Indo-Pacific warming, *Nature*, *491*, 439–443, doi:10.1038/nature11576.
Tselioudis, G., W. Rossow, Y.-C. Zhang, and D. Konsta (2013), Global weather states and their properties from passive and active satellite cloud retrievals, *J. Clim.*, *26*, 7734–7746, doi:10.1175/JCLI-D-13-00024.1.
Tung, K. K., J. Zhou, and C. D. Camp (2008), Constraining model transient climate response using independent observations of solar cycle forcing and response, *Geophys. Res. Lett.*, *35*, L17707, doi:10.1029/2008GL034240.
Vecchi, G. A., and B. J. Soden (2007), Global warming and the weakening of the tropical circulation, *J. Clim.*, *20*(17), 4316–4340.
Wang, B., J. Liu, H.-J. Kim, P. J. Webster, S.-Y. Yim, and B. Xiang (2013), Northern Hemisphere summer monsoon intensified by mega-El Niño/southern oscillation and Atlantic multidecadal oscillation, *Proc. Natl. Acad. Sci. U.S.A.*, *110*(14), 5347–5352, doi:10.1073/pnas.1219405110.
Zelinka, M. D., and D. L. Hartmann (2011), The observed sensitivity of high clouds to mean surface temperature anomalies in the tropics, *J. Geophys. Res.*, *116*, D23103, doi:10.1029/2011JD016459.
Zelinka, M. D., S. A. Klein, K. E. Taylor, T. Andrews, M. J. Webb, J. M. Gregory, and P. M. Forster (2013), Contributions of different cloud types to feedbacks and rapid adjustments in CMIP5, *J. Clim.*, *26*, 5007–5027, doi:10.1175/JCLI-D-12-00555.1.